Article

Double Diffusive Natural Convection in a Square Cavity Filled with a Porous Media and a Power Law Fluid Separated by a Wavy Interface

Lioua Kolsi [1,*] **, Shafqat Hussain** [2]**, Kaouther Ghachem** [3]**, Muhammad Jamal** [4] **and Chemseddine Maatki** [5,6]

[1] Mechanical Engineering Department, College of Engineering, University of Ha'il, Ha'il 81451, Saudi Arabia
[2] Department of Mathematics, Capital University of Science and Technology, Islamabad 44000, Pakistan; shafqat.hussain@cust.edu.pk
[3] Department of Industrial Engineering and Systems, College of Engineering, Princess Nourah bint Abdulrahman University, Riyadh 11671, Saudi Arabia; kgmaatki@pnu.edu.sa
[4] Department of Mathematics & Statistics, PMAS-Arid Agriculture University, Rawalpindi 46300, Pakistan; jamal@uaar.edu.pk
[5] Department of Mechanical Engineering, College of Engineering, Imam Mohammad Ibn Saud Islamic University, Riyadh 11432, Saudi Arabia; casmaatki@imamu.edu.sa
[6] Laboratory of Metrology and Energy Systems, University of Monastir, Monastir 5000, Tunisia
* Correspondence: l.kolsi@uoh.edu.sa

Abstract: This study deals with the influence of a wavy interface separating two layers filled with power law fluid and porous media, respectively. The governing equations are solved using the Finite Element Method (FEM) and the numerical model is validated by comparing with experimental findings. The parameters governing the studied configuration are varied as: Rayleigh number ($10^3 \leq Ra \leq 10^6$), power law index ($0.6 \leq n \leq 1.4$), Darcy number ($10^{-2} \leq Da \leq 10^{-6}$), buoyancy ratio ($0.1 \leq N \leq 10$) and Lewis number ($1 \leq Le \leq 10$). It is inferred that the temperature gradient increases by augmenting the Rayleigh number, as the flow is observed from the vertical to horizontal direction in both layers. Constant enhancement in the heat and mass transfer is also observed by enriching the buoyancy effect. Moreover, the average Nusselt and Sherwood numbers decline by increasing the width of the porous layer.

Keywords: non-Newtonian fluid; layers; double diffusive; natural convection; FEM

1. Introduction

The double diffusion is a phenomenon that occurs in several engineering and industrial applications such as pulp paper, oil drilling, heat removal, heat storage, and food processing [1–6]. There are relatively few works that have been conducted on non-Newtonian fluid, instead of Newtonian fluid. Al-Amir et al. [7] reported the impact of the Prandtl number on the natural convection in cavity-containing non-Newtonian and nanofluid porous mediums, which are separated by the sinusoidal interface. It has been realized that the average Nusselt number rises by enhancing the Darcy and Prandlt number, and reduces by enriching the power law index. Alsabery et al. [8] examined the trapezoidal-shaped cavity including two layers (porous and non-Newtonian). The results confirmed that the flow rises remarkably when using silver nanofluid, and the effectiveness of heat transfer is perceived by varying the angle of inclination. The impact of wavy interfaces on the natural convection in non-Darcy porous cavities is studied by Nguyen et al. [9], using the incompressible smoothed particle hydrodynamics (ISPH) method. The results indicated that the average Nusselt number decreases by increasing the amplitude and undulation number of the interface separating the layers. Alsabery et al. [10] performed a numerical study to investigate the effect of the inclination on natural convection in a cavity filled with a porous media and a non-Newtonian fluid. The findings showed that convection is

more intense for lower values of power law index. Power law fluids have attracted the researchers due to their importance in several engi-neering applications [11]. More related studies can be found in References [12–16]. The natural convection in porous layers has been studied Al-Srayyih et al. [17] using Galerkin Finite Element Method (GFEM). It was found that the enhancement of the heat transfer occurs using nanofluids. Barnoon et al. [18] investigated the coupled radiation-convection in a cavity filled with a non-Newtonian fluid and equipped with internal obstacles. The authors concluded that the tilt angle has an important effect of the values of Nusselt number. Jabber et al. [19] investigated the 2D natural convection in an enclosure filled with a porous medium saturated with a anofluid and equipped by wavy interfaces. The authors mentioned that power law index causes a reduction of the heat transfer rate. The effect of a power law fluid on natural convection in a cavity having wavy wall has been investigated by Chen et al. [20]. It was shown that the rate of heat transfer of pseudoplastic fluid is better compared to Newtonian fluid. Kefayati et al. [21] applied LBM to realize the behavior of non-Newtonian fluid under natural convection; a uniform magnetic field is also applied in this study. The results indicated that the heat transfer increases with the power law index and decreases with the Hartman number. Saleh et al. [22] studied a differentially heated cavity equipped with rotating obstacles. The results showed that the values of Nusselt number remain constant at $L/D > 0.77$. Other research papers related to the effect of separating interfaces in cavities are reported [23–28]. Turan et al. [29] studied the natural convection of a non-Newtonian fluid. They investigated the influence of the Prandtl number, and proposed new correlations for the Nusselt number for Newtonian and non-Newtonian fluids.

Based on the above-described literature review, and to the best of the authors' knowledge, there is currently no published work on wavy interfaces in square cavities filled with two layers (non-Newtonian and porous (Newtonian)). The applications of the current study are in engineering and industry. We can further study this by increasing the layers. The effect of various controlled parameters, such as the Rayleigh number, power law index, Darcy number, buoyancy ratio, and Lewis number, is examined in detail.

2. Problem Formulation

The problem configuration is schematically illustrated in (Figure 1). It consists of 2D double-diffusive convection in a cavity containing two fluid layers (non-Newtonian and porous Newtonian fluid), which are separated by a sinusoidal wall. L and H represent the length and height of the cavity, respectively. θ_h and C_h are the high temperature and concentration at the left wall, respectively. Similarly, θ_c and C_c are the low temperature and concentration at the right wall, respectively. The remaining horizontal walls are considered to be adiabatic. The flow is considered to be laminar, steady, and incompressible, with the application of the Darcy–Brinkman–Forchheimer model.

The wavy interface is derived from the following equation:

$$X = Hp + A\ Sin\left(\frac{2\pi K}{L}Y + \varphi\right) \tag{1}$$

where Hp and A represent the width of the porous layer and the amplitude, respectively. φ denotes the phase shift, which is taken as $\frac{\pi}{2}$.
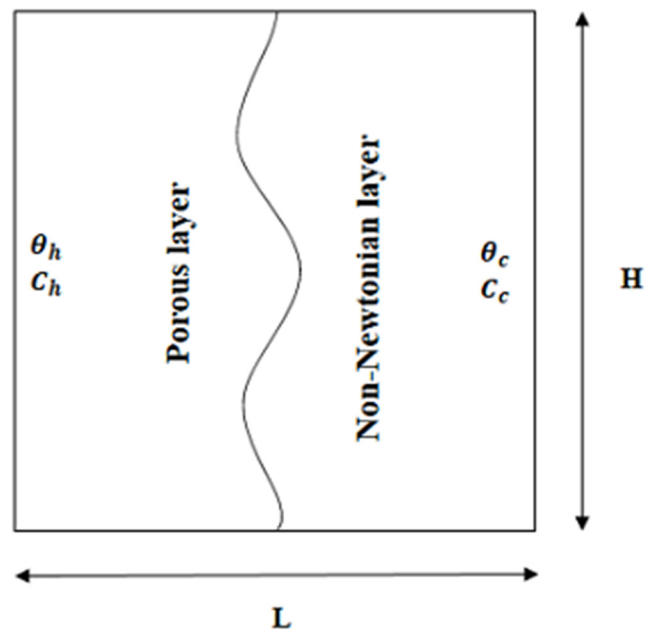
Figure 1. Schematic diagram.

3. The Governing Equations

Under the above-considered assumptions, the dimensionless systems of the equations for the fluid region and porous layer are written as follows [30–36]:

For the non-Newtonian fluid layer:

$$\frac{\partial U}{\partial X} + \frac{\partial V}{\partial Y} = 0 \tag{2}$$

$$U\frac{\partial U}{\partial X} + V\frac{\partial U}{\partial Y} = -\frac{\partial P}{\partial X} + \frac{Pr}{\sqrt{Ra}}\left[2\frac{\partial}{\partial X}\left(\frac{\mu_a}{M}\frac{\partial U}{\partial X}\right) + \frac{\partial}{\partial Y}\left(\frac{\mu_a}{M}\left(\frac{\partial U}{\partial Y} + \frac{\partial V}{\partial X}\right)\right)\right] \tag{3}$$

$$U\frac{\partial V}{\partial X} + V\frac{\partial V}{\partial Y} = -\frac{\partial P}{\partial Y} + \frac{Pr}{\sqrt{Ra}}\left[2\frac{\partial}{\partial Y}\left(\frac{\mu_a}{M}\frac{\partial V}{\partial Y}\right) + \frac{\partial}{\partial X}\left(\frac{\mu_a}{M}\left(\frac{\partial U}{\partial Y} + \frac{\partial V}{\partial X}\right)\right)\right] + Pr(\theta + NC) \tag{4}$$

$$U\frac{\partial \theta}{\partial X} + V\frac{\partial \theta}{\partial Y} = \frac{1}{\sqrt{Ra}}\left(\frac{\partial^2 \theta}{\partial X^2} + \frac{\partial^2 \theta}{\partial Y^2}\right) \tag{5}$$

$$U\frac{\partial C}{\partial X} + V\frac{\partial C}{\partial Y} = \frac{1}{Le\sqrt{Ra}}\left(\frac{\partial^2 C}{\partial X^2} + \frac{\partial^2 C}{\partial Y^2}\right) \tag{6}$$

$$\mu_a = M\left\{2\left[\left(\frac{\partial U}{\partial X}\right)^2 + \left(\frac{\partial V}{\partial Y}\right)^2\right] + \left(\frac{\partial V}{\partial X} + \frac{\partial U}{\partial Y}\right)^2\right\}^{\frac{n-1}{2}} \tag{7}$$

where N is the buoyancy ratio and n is the power law index.

The following also applies:

$$Pr = \frac{\mu_a}{\rho\alpha} \tag{8}$$

$$Ra = \frac{\rho\beta g_y L^3(T_H - T_C)}{\mu_a \alpha} \tag{9}$$

$$Le = \frac{a_e}{D} \tag{10}$$

For the porous fluid layer:

$$\frac{\partial \overline{U}}{\partial X} + \frac{\partial \overline{V}}{\partial Y} = 0 \tag{11}$$

$$\overline{U}\frac{\partial \overline{U}}{\partial X} + \overline{V}\frac{\partial \overline{U}}{\partial Y} = -\frac{\partial \overline{P}}{\partial X} + \frac{Pr_m}{\sqrt{Ra_m}}\left(\frac{\partial^2 \overline{U}}{\partial X^2} + \frac{\partial^2 \overline{U}}{\partial Y^2}\right) - \frac{Pr_m \, \overline{U}}{Da_m \, \sqrt{Ra_m}} - \frac{\overline{U} \, |\overline{U}|}{\sqrt{Da_m}} \frac{1.75}{\sqrt{150}} \tag{12}$$

$$\overline{U}\frac{\partial \overline{V}}{\partial X} + \overline{V}\frac{\partial \overline{V}}{\partial Y} = -\frac{\partial \overline{P}}{\partial Y} + \frac{Pr_m}{\sqrt{Ra_m}}\left(\frac{\partial^2 \overline{V}}{\partial X^2} + \frac{\partial^2 \overline{V}}{\partial Y^2}\right) + Pr_m\left(\overline{\theta} + N\overline{C}\right) - \frac{Pr_m \, \overline{V}}{Da_m \, \sqrt{Ra_m}} - \frac{\overline{V} \, |\overline{U}|}{\sqrt{Da_m}} \frac{1.75}{\sqrt{150}} \tag{13}$$

$$\overline{U}\frac{\partial \overline{\theta}}{\partial X} + \overline{V}\frac{\partial \overline{\theta}}{\partial Y} = \frac{1}{\sqrt{Ra_m}}\left(\frac{\partial^2 \overline{\theta}}{\partial X^2} + \frac{\partial^2 \overline{\theta}}{\partial Y^2}\right) \tag{14}$$

$$\overline{U}\frac{\partial \overline{C}}{\partial X} + \overline{V}\frac{\partial \overline{C}}{\partial Y} = \frac{1}{Le \, \sqrt{Ra_m}}\left(\frac{\partial^2 \overline{C}}{\partial X^2} + \frac{\partial^2 \overline{C}}{\partial Y^2}\right) \tag{15}$$

where the following parameters are entered in the above problem:

$$Da = \frac{K}{L^2} \tag{16}$$

The relationship among the actual and modified Prandtl, Rayleigh and Darcy numbers can be written as follows: $Pr_m = Pr \in$, $Ra_m = Ra \in$ and $Da_m = \frac{Da}{\in}$.

The boundary conditions of the proposed problem in the corresponding regions are as follows:

$\overline{U} = 0, \overline{\theta} = 1, \overline{V} = 0, \overline{C} = 1$ (left wall)
$U = 0, \theta = 0, V = 0, C = 0$ (right wall)
$\frac{\partial \overline{\theta}}{\partial Y} = \frac{\partial \overline{C}}{\partial Y} = 0, \overline{U} = \overline{V} = 0$ and $\frac{\partial \theta}{\partial Y} = \frac{\partial C}{\partial Y} = 0, U = V = 0$ (top/bottom walls)

The numbers on the vertical hot wall are given as follows:

$$Nu = \left(-\frac{\partial \overline{\theta}}{\partial X}\right)_{X=0} : \text{ Nusselt number (local)} \tag{17}$$

$$Sh = \left(-\frac{\partial \overline{C}}{\partial X}\right)_{X=0} : \text{ Sherwood number (local)} \tag{18}$$

$$Nu_{avg} = \int_0^1 Nu \, dY : \text{ Nusselt number (average)} \tag{19}$$

$$Sh_{avg} = \int_0^1 Sh \, dY : \text{ Sherwood number (average)} \tag{20}$$

4. Solution Methodology

The mathematical models presented in Equations (2)–(7) and (11)–(15) is solved using the higher order Galerkin finite element method. As a first step, a weak formulation is developed by choosing a suitable test space. Afterwards, a hybrid mesh, consisting of both triangular and quadrilateral elements, is generated to cover the computational domain. A finite element method involving the cubic polynomials (P_3) is implemented to compute the velocity, temperature, and concentration fields, while the pressure is approximated by the quadratic (P_2) finite element space of functions. The stability and robustness of this higher-order pair of FEMs has been tested in [37]. The system of discretized equations is simplified using the adaptive Newton's method. For further details regarding the solver, the reader is referred to [38].
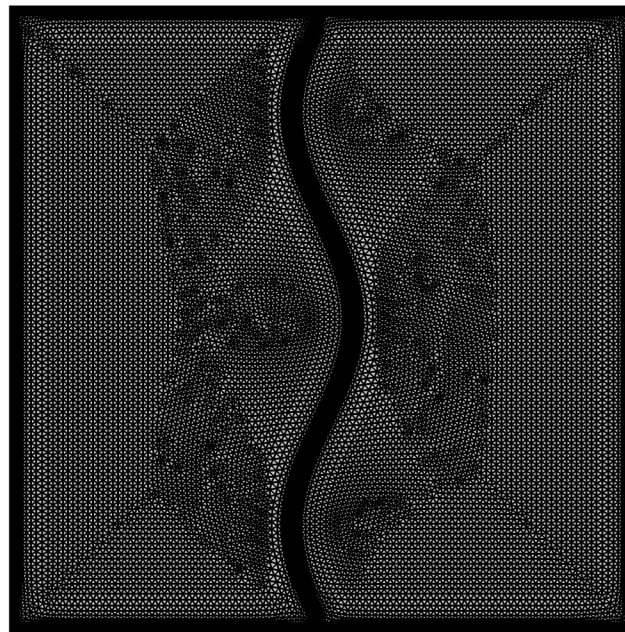
4.1. Grid Convergence

As shown in Table 1, eight number of elements are compared to check the mesh independency at $Gr = 10^5$, $Da = 10^{-3}$, $\epsilon = 0.75$ and $Hp = 0.1$. From this comparison it is clear that the deviations of Nu_{av} and Sh_{av} between the grids G7 and G8 are very small. Thus, for time economy and results accuracy the grid G7 was retained for all the performed simulations. The grid for the proposed computational model is displayed in Figure 2.

Table 1. Convergence of grid analysis.

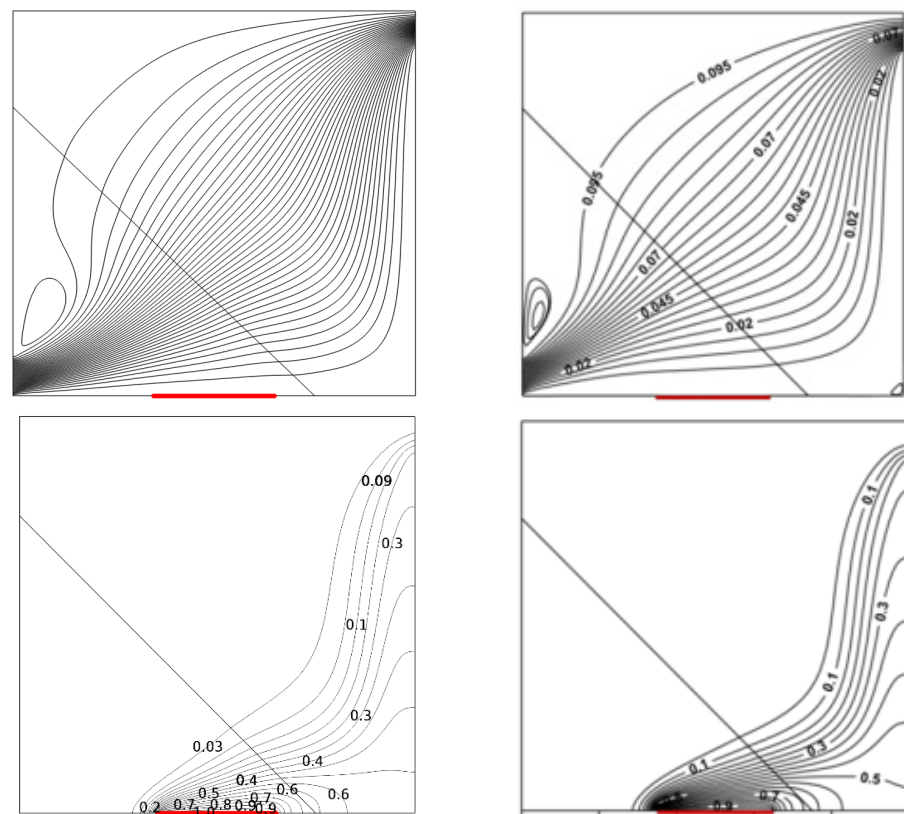| Grid	NEL	DOFs	Nu_{avg}	Sh_{avg}
G1	230	3322	3.428355	5.767679
G2	352	4974	3.418098	5.727896
G3	540	7319	3.420159	5.715686
G4	1006	13007	3.422258	5.703224
G5	1520	19040	3.424014	5.701316
G6	2470	29757	3.424601	5.700223
G7	6544	76933	3.424613	5.698674
G8	16790	192148	3.424915	5.698709

Figure 2. The grid for the proposed model.

4.2. Code Validation

The current results are checked by comparing them to those of Gibanov et al. [39], by evaluating the average Nusselt number under the same conditions. As is shown in Table 2, the error did not exceed 0.36%, which represents good agreement among the two results. Moreover, the numerical code is checked by comparing the isotherms and streamlines with those found by Gibanov et al. [39]. The results of the current numerical model are in concordance with the results of Gibanov et al. [39] (Figure 3).
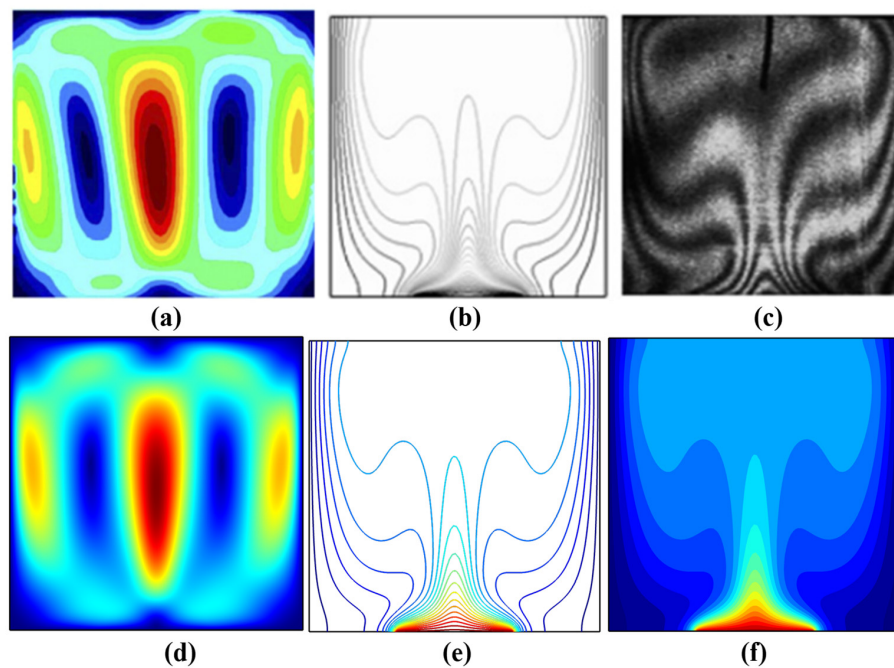
Table 2. Validation of the code of average *Nu* with [39]. Adapted with permission from ref. [39]. Copyright 2017 Springer Nature.

Present Study	[39]	Error
12.57879	12.5335	0.36%
Present Model		Gibanov et al. [39].

Figure 3. Comparison of the flow structure and temperature field with those of Gibanov et al. [39]. Reprinted with permission from ref. [39]. Copyright 2017 Springer Nature.

In addition to the above validation, to strengthen the reliability of the implemented FEM, we also confirmed the validation by comparing it with the experimental study of Corvaro and Paroncini [40], as demonstrated in Figure 4.

Figure 4. Comparison with the results of Corvaro and Paroncini [40] (Reprinted with permission from ref. [40]. Copyright 2007 Elsevier): flow field (experimental in (**a**)), isotherms (numerical in (**b**)), and isotherms (experimental in (**c**)). The corresponding present numerical study is given in (**d**–**f**).

5. Results and Discussion

The results of the different numerical simulation cases are presented by streamlines, isotherms and isoconcentration contours, as well as variations in the local *Nu* and *Sh*, and variations in the average Nu and Sh. All the simulations are performed for the fixed values of $n = 0.6$, $Da = 10^{-3}$, $\epsilon = 1.0$, $Le = 2.5$, $Pr = 1$, $N = 0.1$, $M = 2$, $Hp = 0.5$, $A = 0.05$, and $Ra = 10^5$.

For each case, one parameter is varied. In fact, the results will consecutively present the effect of the variation in the Rayleigh number (*Ra*), power law index (*n*), Darcy number (*Da*), buoyancy number (*N*), and Lewis number (*Le*). Furthermore, the effects of the width of the porous media (*Hp*), the undulation number of interface (*K*), and its amplitude (A) on the average *Nu* and *Sh* are presented for a range of the power law index (*n*), varied from 0.6 to 1.6.

5.1. Impact of Rayleigh Number

Figure 5 presents the effect of the Rayleigh number on the streamlines (left side), isotherms (center), and isoconcentrations (right side). Due to its great effect on the heat transfer rate, the Rayleigh number is varied from 10^3 to 10^6. For a low Rayleigh number ($Ra = 10^3$), the center of the main vortex is located on the non-Newtonian side of the cavity and rotates counterclockwise. By increasing the *Ra* number, the rotation of the main vortex is intensified. Remarkable penetration in the direction of the porous layer is detected, due to the elongation of the main vortex.

As can be observed for $Ra = 10^6$, the intensity of the streamlines occurs at the core of the cavity, indicating an increase in the heat transport, due to the natural convection. Here, it is noticed that the center of the vortex is still on the non-Newtonian side. By increasing the *Ra* number, the behavior of the isotherms is modified, due to the enhancement of the temperature gradient. When the *Ra* number is equal to 10^3, the isotherms are parallel to each other, indicating the domination of the conductive heat transfer mode, but as its value rises, an increase in the temperature gradient is observed. The thermal flow passes from a conductive regime to a convective regime by increasing the *Ra* number. Indeed, the stratification of the isotherms is pronounced when the *Ra* number passes from 10^3 to 10^6. The thermal gradient is more densely packed close to the downside of the hot wall, indicating an important thermal boundary layer. This fact is confirmed by the coordinates of the height of the local Nusselt numbers in Figure 4. The isoconcentration behavior is greatly affected by the increase in the *Ra* numbers, which indicates a progressive move from a diffusive to convective mass transfer. When $Ra = 10^6$, the solutal gradient near the hot wall is important, which indicates the importance of the convective transfer from the non-Newtonian fluid layer to the porous layer.

Figure 6 presents the variation in the local Nu and *Sh* for different *Ra* numbers. The curves prove the high increase in the *Nu* and *Sh* values when the Rayleigh number passes from 10^5 to 10^6. Table 3 presents a comparison between the average Nu and average *Sh* for various Rayleigh numbers, under the same conditions. For $Ra = 10^3$ and $Ra = 10^4$, the *Nu* values are low compared to the other Rayleigh values. This is due to the lower heat exchange between the porous medium layer and the non-Newtonian layer. The maximum values of the average *Nu* and *Sh* numbers confirm the importance of the mass transfer effect on behalf of the heat transfer, especially when the *Ra* numbers increase. This is due to the current case condition, in which the buoyancy number is equal to 0.1.

Table 3. Average *Nu* and *Sh* comparison.

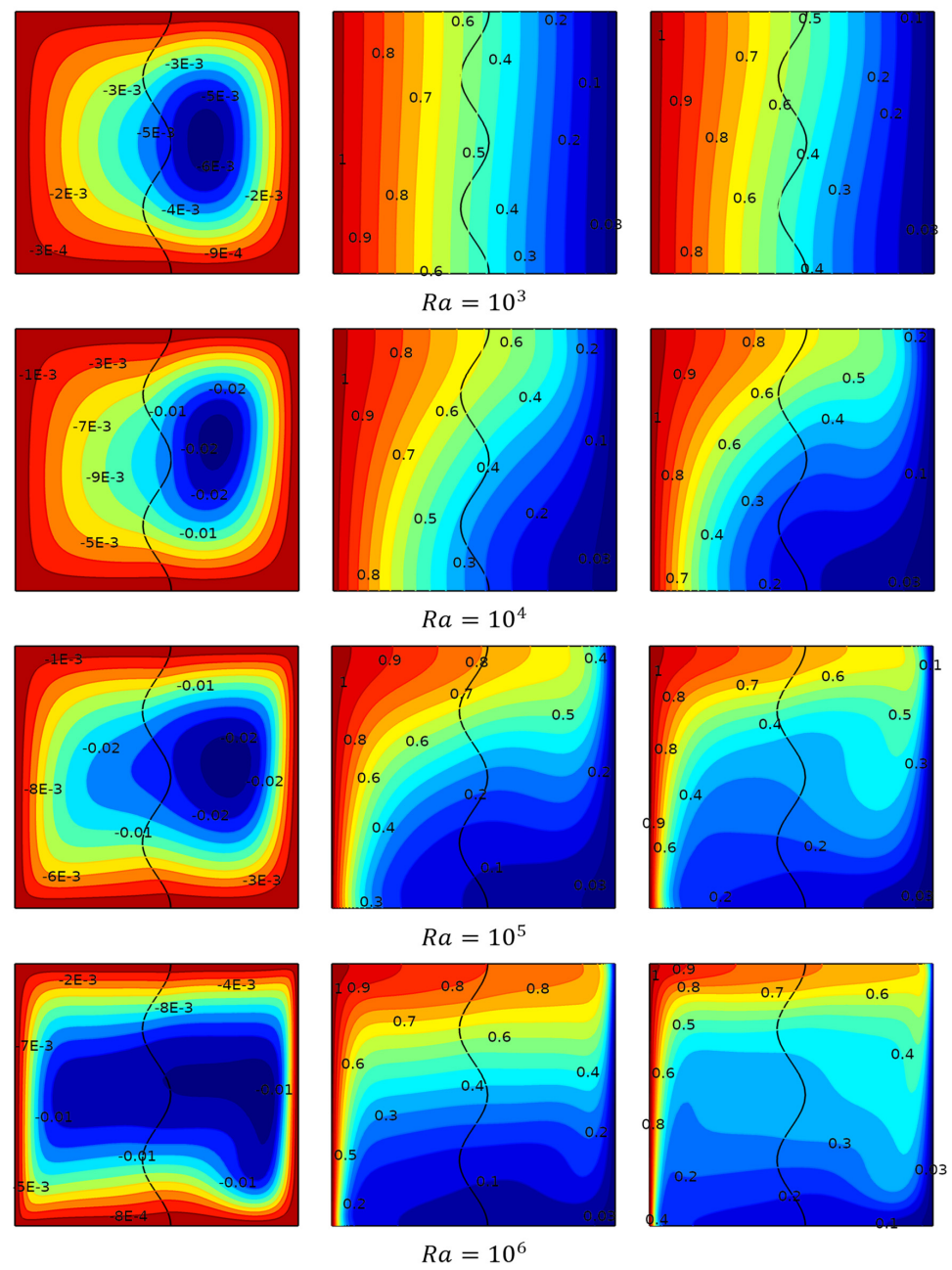|	$Ra = 10^3$	$Ra = 10^4$	$Ra = 10^5$	$Ra = 10^6$
Nu_{avg}	1.003544	1.294151	3.425027	8.530151
Sh_{avg}	1.021881	2.017548	5.699002	13.07502

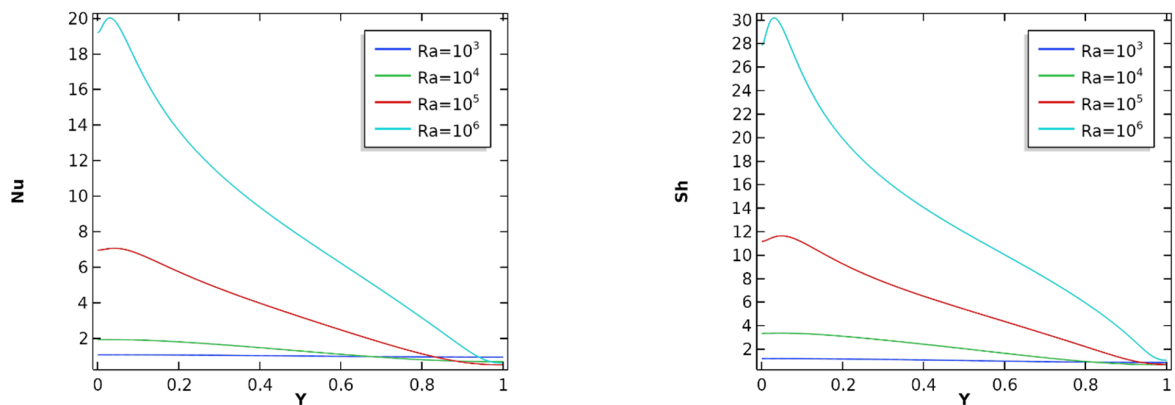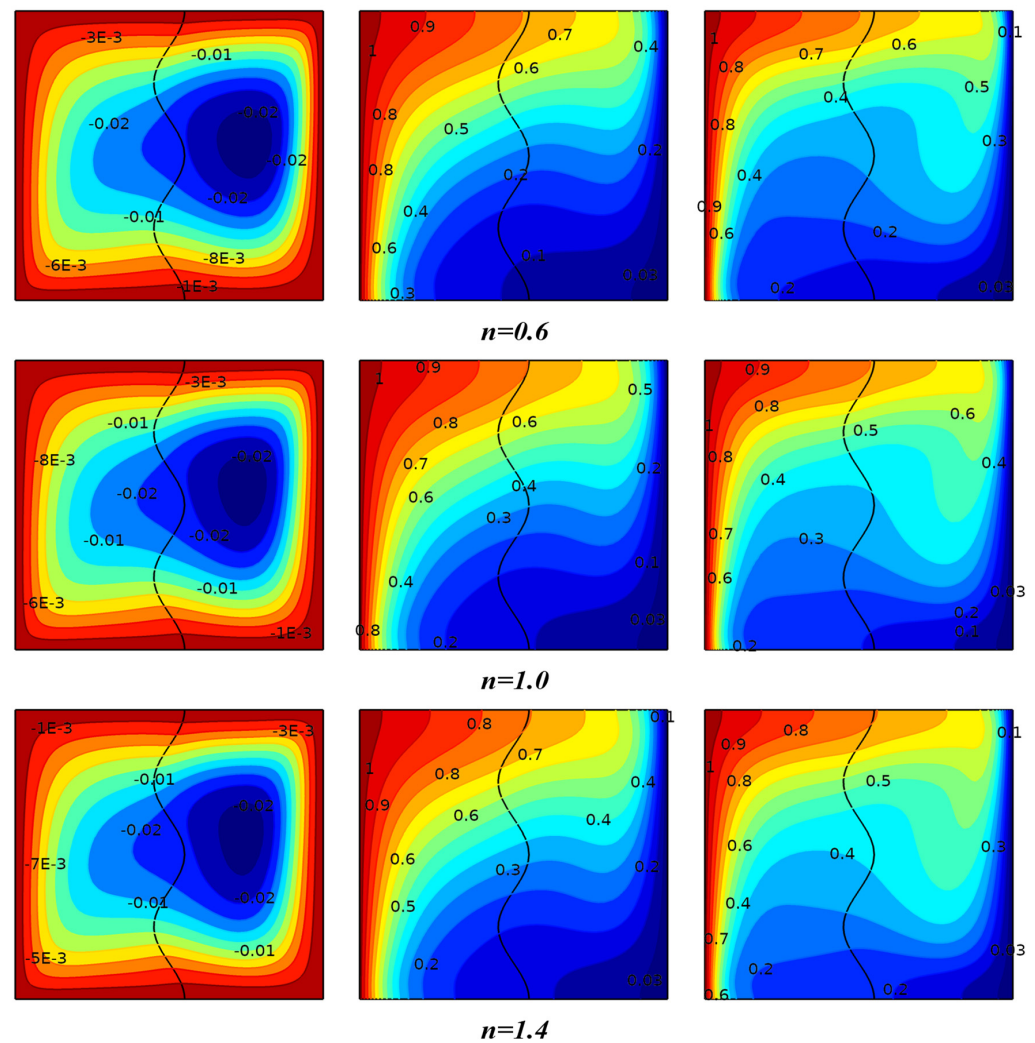**Figure 5.** Streamlines (column 1), isotherms (column 2), and isoconcentration (column 3).

Figure 6. Variation in local *Nu* and *Sh*.

5.2. Impact of Power Law Index

Figure 7 presents the streamlines (left side), the isotherms (center), and the isoconcentration (right side). By definition, the power law index affects the heat generation and, consequently, the viscosity. The expected results need to demonstrate the regression of the heat transfer and show a great impact on the mass transfer between the two layers. As the power law index rises, the intensity and movement of the streamlines are slightly affected in the cavity, which means that the energy required to rotate the vortex decreases. This fact is explained further by plotting the variation in the local *Nu* and *Sh*, and calculating their mean values at the hot wall (Table 4). Regardless of the fact that they exhibit the same behavior, it is clear in Figure 8 that the variation in the local *Nu* and *Sh* drops by increasing the n values.

Table 4. Average *Nu* and *Sh* comparison.

	n = 0.6	*n* = 0.8	*n* = 1	*n* = 1.2	*n* = 1.4
Nu_{avg}	3.424915	3.338505	3.272834	3.221858	3.181187
Sh_{avg}	5.698709	5.519309	5.383465	5.278273	5.194299

n=0.6

n=1.0

n=1.4

Figure 7. Streamlines (column 1), isotherms (column 2), and isoconcentration (column 3).
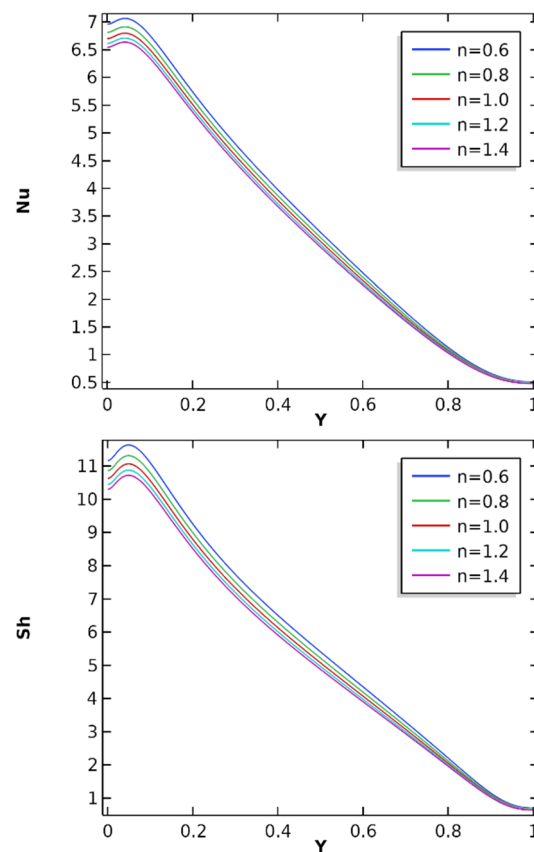
Figure 8. Variation in local *Nu* and *Sh*.

5.3. Impact of Darcy Number

Figure 9 presents the effect of the Darcy number (*Da*) variation on the streamlines, isotherms, and isoconcentrations, while the other parameters are constant. When the *Da* is equal to 10^{-6} and 10^{-5}, the streamlines are localized in the non-Newtonian zone, which indicates that no exchange is performed between the porous and non-Newtonian layers. The isothermal and isoconcentration lines are parallel in the porous zone, compared to the non-Newtonian zone. By increasing the Darcy numbers, the spread of the streamline through the wavy interface is increasingly developed. The thermal and solutal gradient near the downside of the hot wall is noticed, due to the rise in the Darcy numbers. The results show that for $Da = 10^{-2}$, thermal stratification takes place and solutal distortion appears in the core cavity, since the value of the Darcy number increases to 10^{-3}.

The variation in the local *Nu* and *Sh* for different Darcy numbers (*Da*) is shown in Figure 10. For low values of Darcy numbers (10^{-6} and 10^{-5}), the heat and mass transfer are almost constant and at low levels. A slight increase is detected when the Darcy number is equal to 10^{-4}. A noticeable increase in the heat and mass transfer effect takes place for $Da = 10^{-3}$ and 10^{-2}, which is described by the rise in the vortex rotation intensity through the two sides of the wavy interface. Table 5 presents the evolution of the average *Nu* and *Sh* for the various values of *Da*, when $Ra = 10^5$, $Da = 10^{-3}$, $\epsilon = 0.75$, and $Hp = 0.1$. The great increase in the heat and mass transfer values can be deduced by the increase in the diffusivity of the fluid flow through the interface to the porous medium.

Table 5. Average *Nu* and *Sh* comparison.

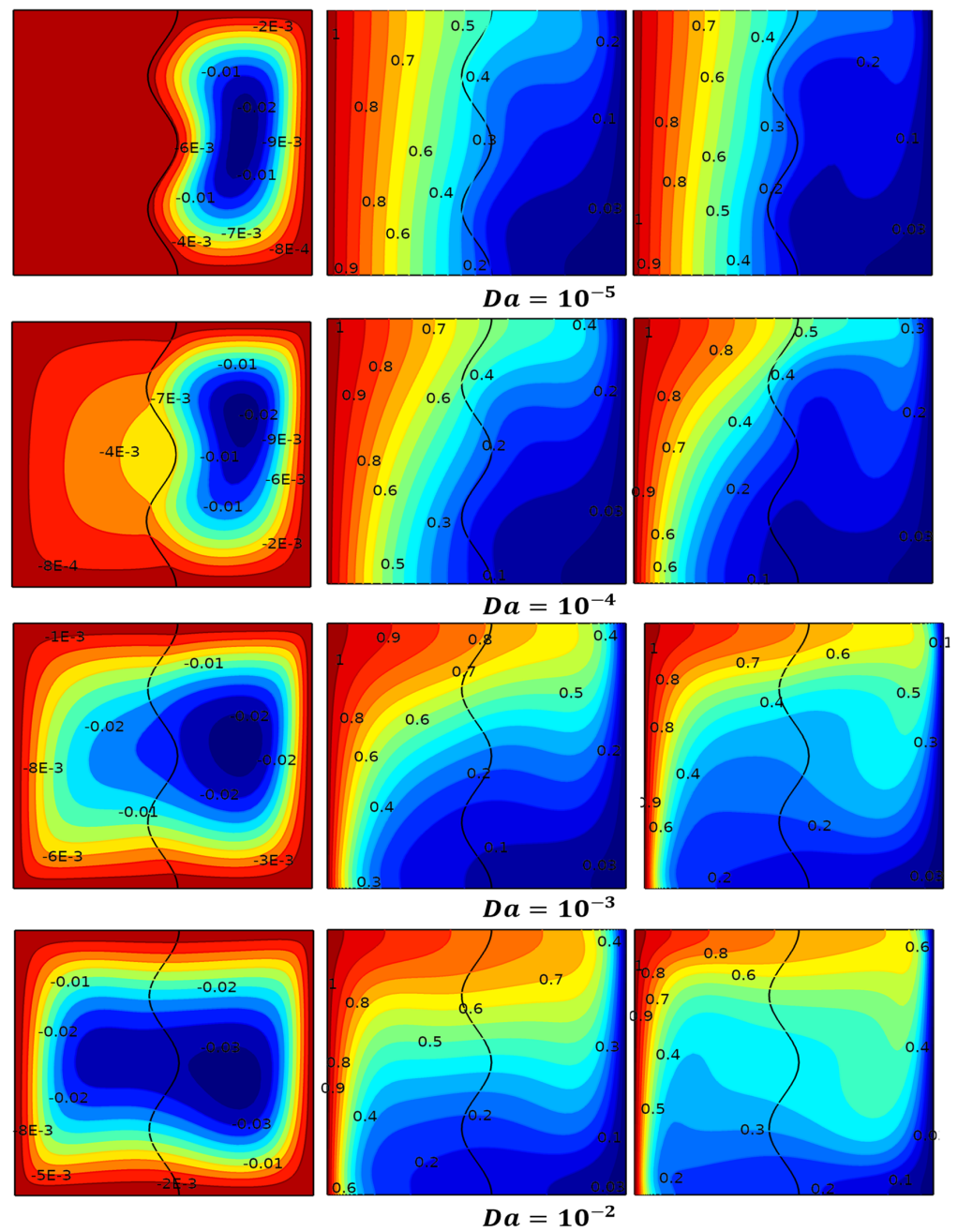|	$Da = 10^{-6}$	$Da = 10^{-5}$	$Da = 10^{-4}$	$Da = 10^{-3}$	$Da = 10^{-2}$
Nu_{avg}	1.3556	1.373742	1.652894	3.425139	4.703467
Sh_{avg}	1.537805	1.582851	2.50985	5.699306	7.181993

Figure 9. Streamlines (column 1), isotherms (column 2), and isoconcentration (column 3).
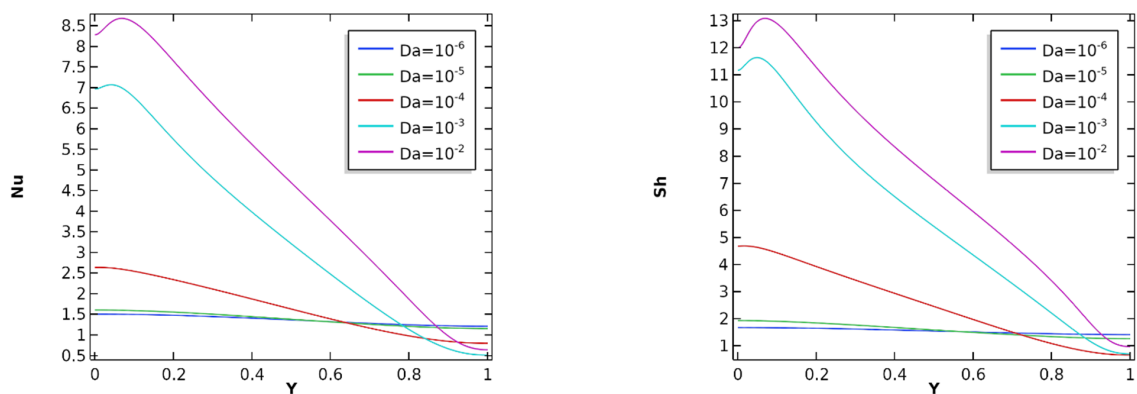

Figure 10. Variation in local *Nu* and *Sh*.

5.4. Impact of Buoyancy Ratio

The effect of the variation in the buoyancy number N from 0.1 to 10, when the other values remain constant, is presented in Figure 11. The behavior of the streamlines is similar to the Ra variation cases. The main cell is lengthened to the whole cavity space by increasing the N values, although the center of the vortex is still localized in the non-Newtonian zone. The thermal gradient is densely packed near the downside of the hot wall in the porous media zone by the increase in the N values, which results in intensification of the heat transfer through the interface. Moreover, the solutal gradient is tightened near the downside of the hot wall and the topside of the cold wall, and stratification of the isoconcentrations takes place in the core region of the cavity.

These behaviors could be explained by the profiles of the local Nu and Sh in Figure 12, and their average values in Table 6. The enhancement of the heat and mass transfer through the interface is measured by increasing the buoyancy effect.
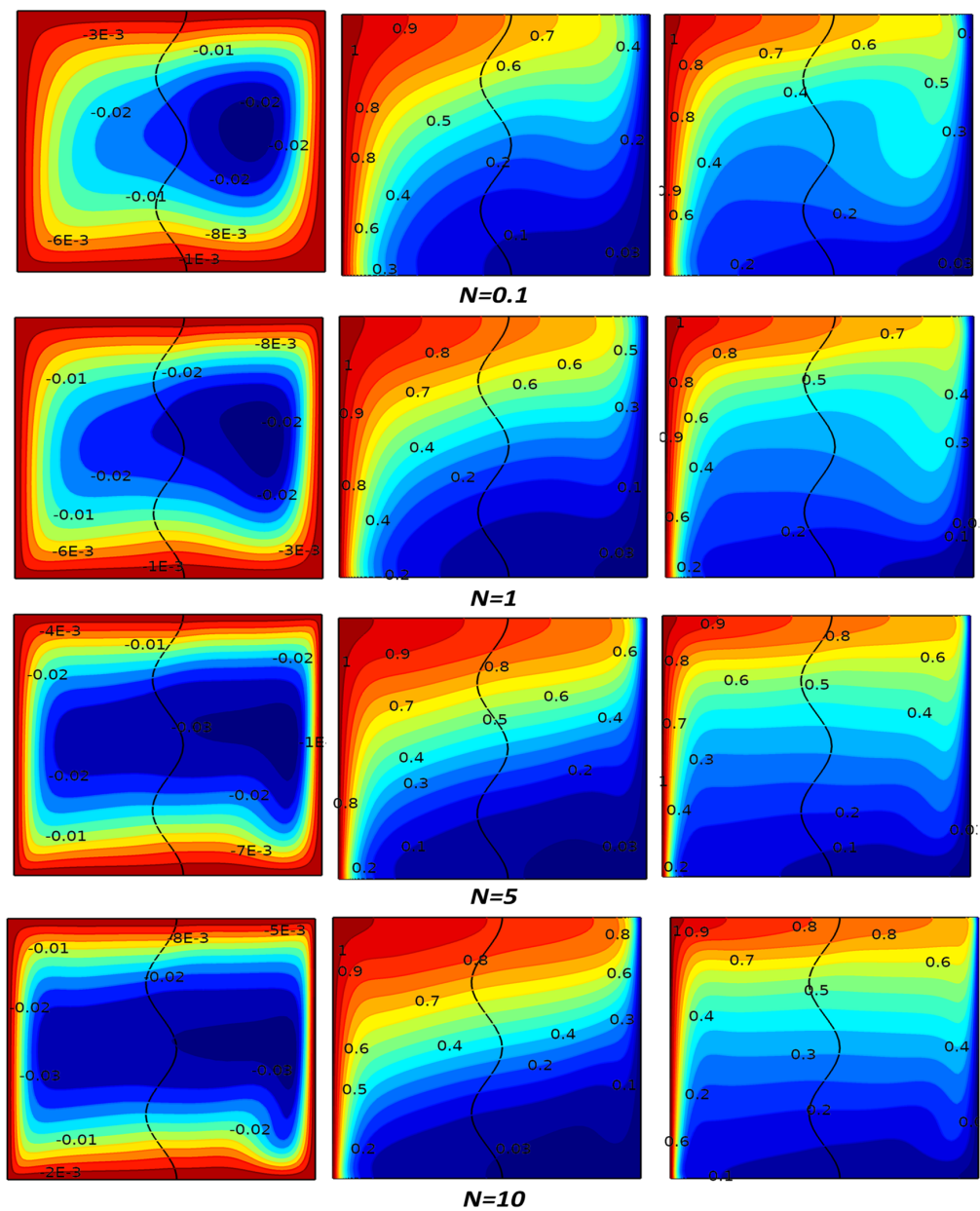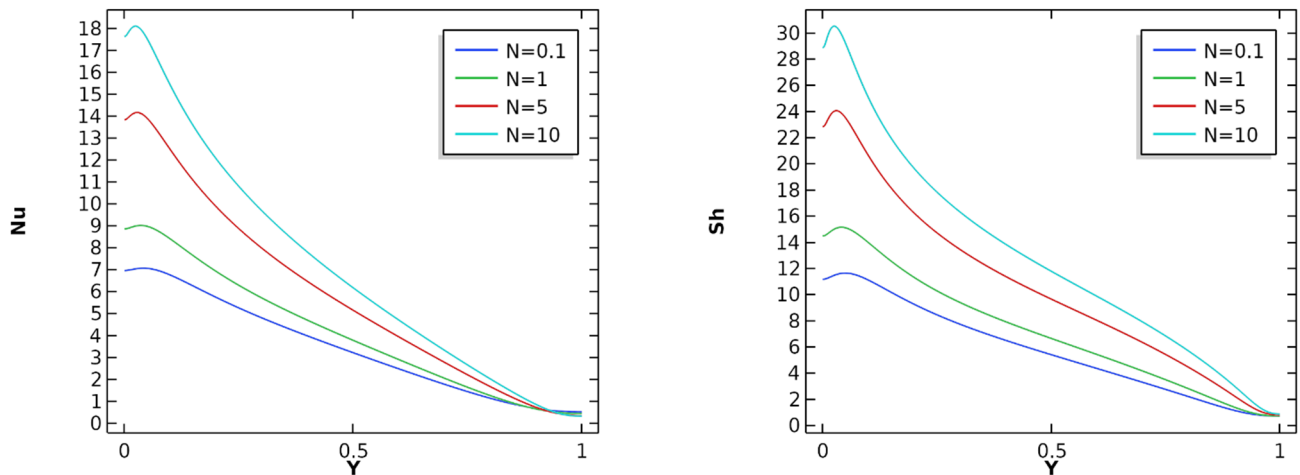

Figure 11. Streamlines (column 1), isotherms (column 2), and isoconcentration (column 3).

Table 6. Average *Nu* and *Sh* comparison.

	N = 0.1	**N = 1**	**N = 5**	**N = 10**
Nu_{avg}	3.424915	4.102939	5.831249	7.130527
Sh_{avg}	5.698709	7.080791	10.47675	12.8777

Figure 12. Variation in local *Nu* and *Sh*.

5.5. Impact of Lewis Number

Figure 13 indicates the streamlines at the left side, the isotherms at the center, and the isoconcentration at the right side. It can be observed that there is not a significant change in the streamline (left side), isotherm (center), and isoconcentration (right side) contours by enhancing the Lewis number for both layers. This is confirmed by Figure 14, where the behavior of the local Nu is almost the same for different values of Lewis number. On the other hand, the local *Sh* is enriched by increasing the Lewis number. The particular reason for this minor change in these results is the small value of the buoyancy ratio ($N = 0.1$). Furthermore, it is observed that there is a minor effect of concentration in the momentum equation. Table 7 depicts the trend of the average *Nu* and *Sh* for different Lewis numbers (*Le*), which reflects the minor decline in the local Nusselt number as the Lewis number rises, but the average Sherwood numbers increase considerably.

Table 7. Average *Nu* and *Sh* comparison.

	Le = 1	**Le = 2.5**	**Le = 5**	**Le = 10**
Nu_{avg}	3.483756	3.425136	3.389914	3.366655
Sh_{avg}	3.48395	5.699383	7.703609	10.18238

In the next portion of this discussion, some plots of the average *Nu* and *Sh* are drawn on the power law index. Figure 15 indicates that the average *Nu* and *Sh* decline with an increase in the width of the porous layer with power law indices. The behavior of the average *Nu* and *Sh* with the undulation parameter and amplitude of the interface is shown in Figures 16 and 17, respectively. It is visualized, in both figures, that the results switch towards the decline direction, by increasing the values of *K* and *A*, correspondingly.
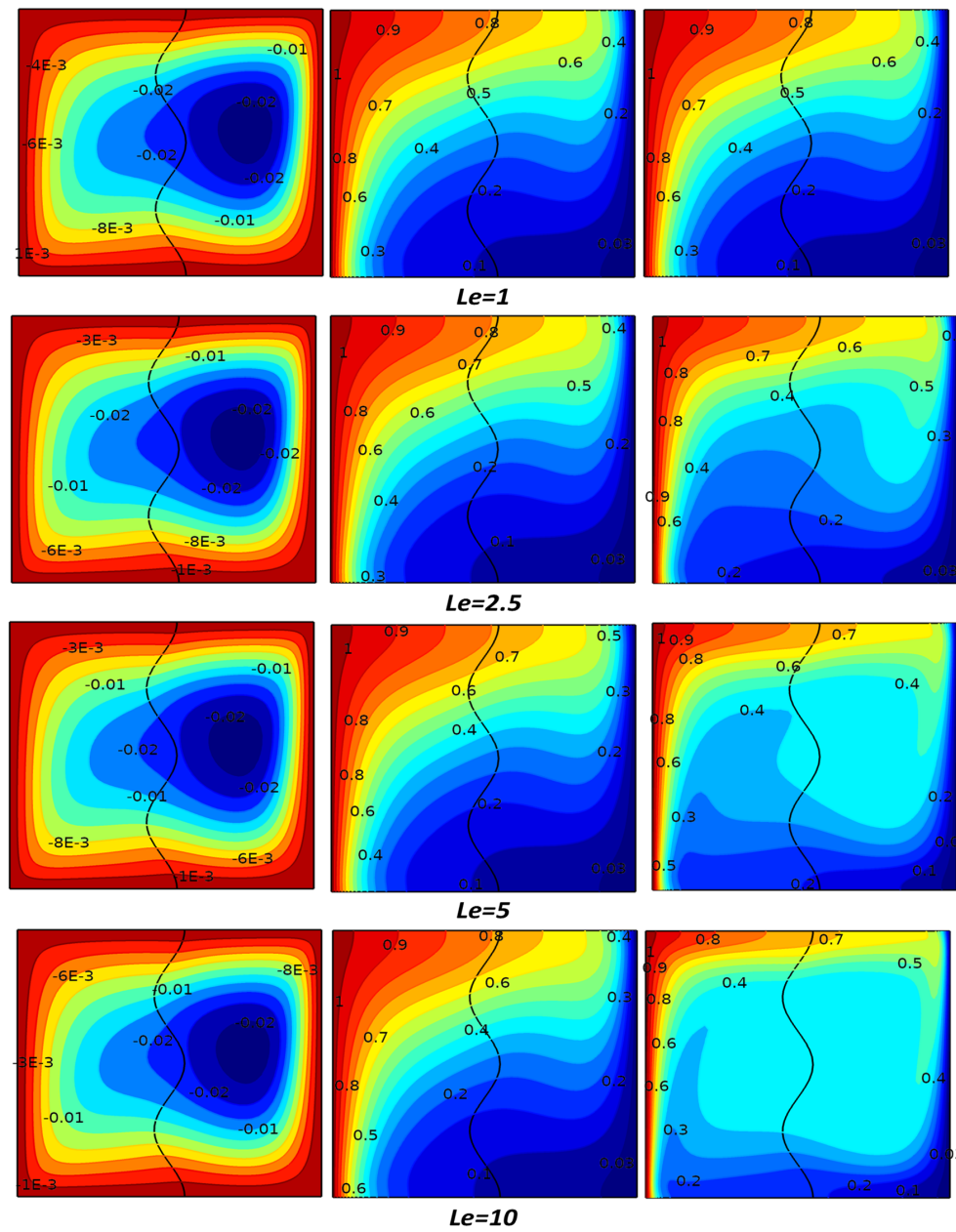
Figure 13. Streamlines (column 1), isotherms (column 2), and isoconcentration (column 3).
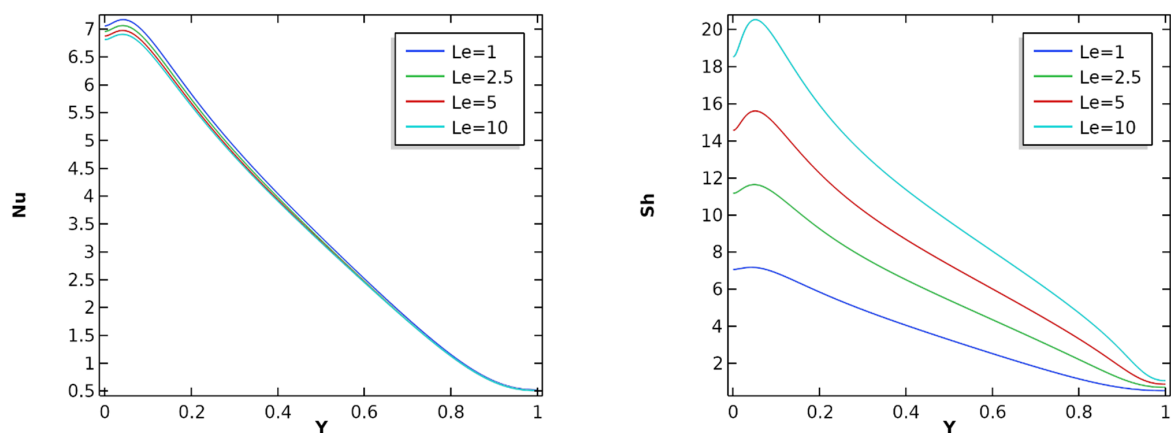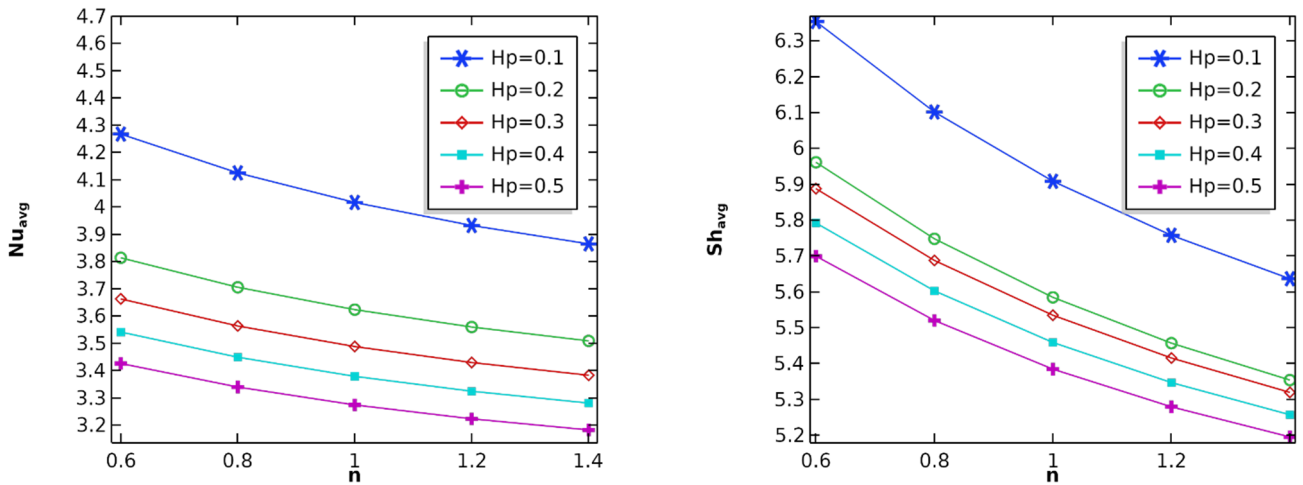

Figure 14. Variation in local *Nu* and *Sh*.
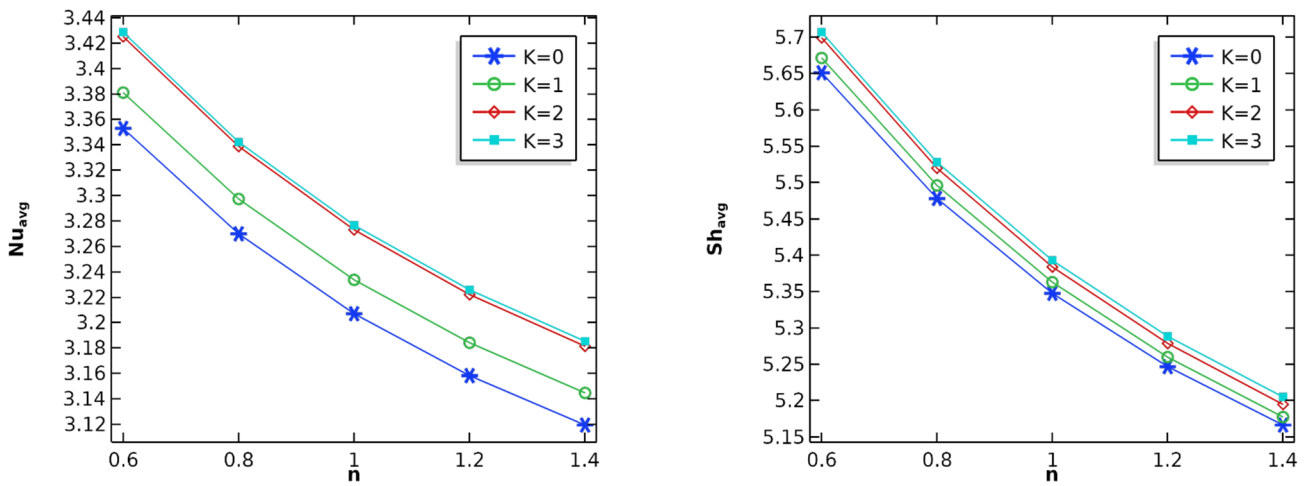
Figure 15. Impact of average *Nu* and *Sh*.

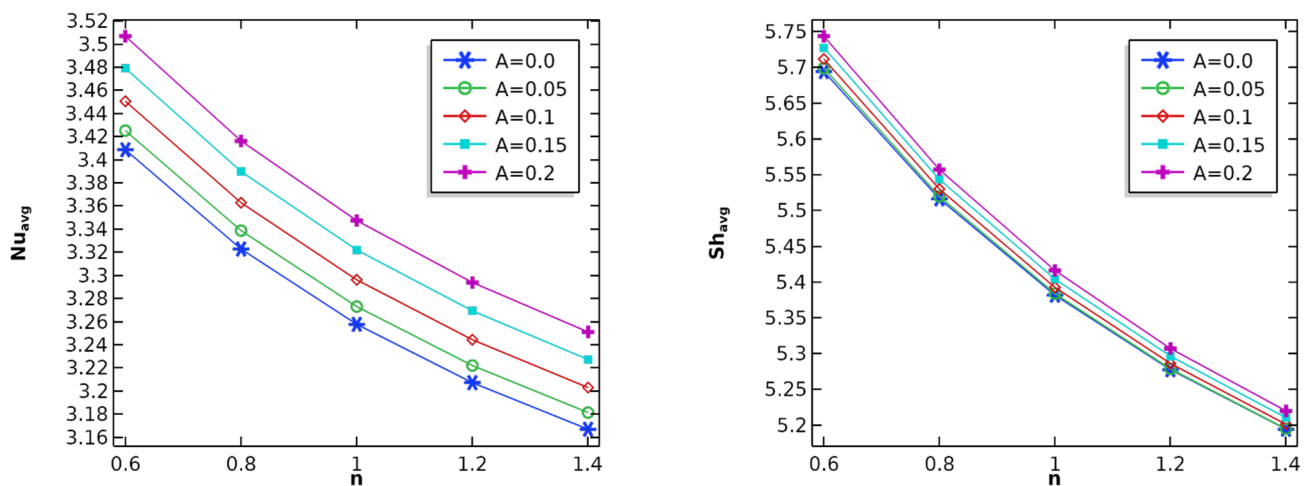**Figure 16.** Impact of average *Nu* and *Sh*.

Figure 17. Impact of average *Nu* and *Sh*.

6. Conclusions

Double-diffusive natural convection has been investigated in a 2D cavity, composed of two layers (non-Newtonian and porous), separated by a wavy interface, using FEM. The

effects of the Rayleigh number, power law index, Darcy number, buoyancy ratio, and Lewis number are studied. The main conclusions can be summarized as follows:

- The temperature gradient rises by augmenting the Rayleigh number, as the flow is observed from the vertical to horizontal direction in both layers of the cavity, which seems to be a remarkable change in heat transfer. Similar behavior is observed in the concentration case.
- By increasing the values of the power law indices, a decline in the average Nu and *Sh* is observed.
- When Da 10^{-6} to 10^{-5}, the streamlines are localized in the non-Newtonian zone, which may indicate that no exchange is observed between the porous and non-Newtonian layers. By increasing the value of Da, the wavy interface is changed.
- Constant enhancement in heat and mass transfer is noticed in a wavy interface by enriching the buoyancy effect.
- The local Nu is almost the same for different values of Lewis number. On the other hand, the local Sh is enriched by increasing the Lewis number.
- The average Nusselt and Sherwood numbers decline by increasing the width of the porous layer with power law indices.
- It is visualized, in both figures, that the average Nu and Sh move towards the decline direction, by increasing the values of K and A, correspondingly.

References

1. Kefayati, G.; Tang, H. Three-dimensional Lattice Boltzmann simulation on thermosolutal convection and entropy generation of Carreau-Yasuda fluids. *Int. J. Heat Mass Transf.* **2019**, *131*, 346–364. [CrossRef]
2. Xin, S.; Le Quéré, P.; Tuckerman, L.S. Bifurcation analysis of double-diffusive convection with opposing horizontal thermal and solutal gradients. *Phys. Fluids* **1998**, *10*, 850–858. [CrossRef]
3. Sezai, I.; Mohamad, A.A. Double diffusive convection in a cubic enclosure with opposing temperature and concentration gradients. *Phys. Fluids* **2000**, *12*, 2210–2223. [CrossRef]
4. Kuznetsov, G.V.; Sheremet, M.A. A numerical simulation of double diffusive conjugate natural convection in an enclosure. *Int. J. Therm. Sci.* **2011**, *50*, 1878–1886. [CrossRef]
5. Khezzar, L.; Siginer, D.; Vinogradov, I. Natural convection of power law fluids in inclined cavities. *Int. J. Therm. Sci.* **2012**, *53*, 8–17. [CrossRef]
6. Ali, L.; Ali, B.; Liu, X.; Ahmed, S.; Shah, M.A. Analysis of bio-convective MHD Blasius and Sakiadis flow with Cattaneo-Christov heat flux model and chemical reaction. *Chin. J. Phys.* 2021; in press. [CrossRef]
7. Al-Amir, Q.; Ahmed, S.Y.; Hamzah, H.K.; Ali, F.H. Effects of Prandtl Number on Natural Convection in a Cavity Filled with Silver/Water Nanofluid-Saturated Porous Medium and Non-Newtonian Fluid Layers Separated by Sinusoidal Vertical Interface. *Arab. J. Sci. Eng.* **2019**, *44*, 10339–10354. [CrossRef]
8. Alsabery, A.; Chamkha, A.; Hussain, S.; Saleh, H.; Hashim, I. Heatline visualization of natural convection in a trapezoidal cavity partly filled with nanofluid porous layer and partly with non-Newtonian fluid layer. *Adv. Powder Technol.* **2015**, *26*, 1230–1244. [CrossRef]
9. Nguyen, M.T.; Aly, A.; Lee, S.-W. Effect of a wavy interface on the natural convection of a nanofluid in a cavity with a partially layered porous medium using the ISPH method. *Numer. Heat Transf. Part A Appl.* **2017**, *72*, 68–88. [CrossRef]

10. Alsabery, A.; Hussain, S.; Saleh, H.; Hashim, I. Inclination angle effect on natural convection in a square cavity partially filled with non-Newtonian fluids layer. *AIP Conf. Proc.* **2015**, *1678*, 060007.

11. Bin Kim, G.; Hyun, J.M.; Kwak, H.S. Transient buoyant convection of a power-law non-Newtonian fluid in an enclosure. *Int. J. Heat Mass Transf.* **2003**, *46*, 3605–3617. [CrossRef]

12. Wu, W.-T.; Massoudi, M. Recent Advances in Mechanics of Non-Newtonian Fluids. *Fluids* **2020**, *5*, 10. [CrossRef]

13. Lamsaadi, M.; Naimi, M.; Hasnaoui, M.; Mamou, M. Natural Convection in a Vertical Rectangular Cavity Filled with a Non-Newtonian Power Law Fluid and Subjected to a Horizontal Temperature Gradient. *Numer. Heat Transf. Part A Appl.* **2006**, *49*, 969–990. [CrossRef]

14. Lamsaadi, M.; Hasnaoui, M. Natural convection of non-Newtonian power law fluids in a shallow horizontal rectangular cavity uniformly heated from below. *Heat Mass Transf.* **2005**, *41*, 239–249. [CrossRef]

15. Alsabery, A.I.; Chamkha, A.J.; Saleh, H.; Hashim, I. Natural Convection Flow of a Nanofluid in an Inclined Square Enclosure Partially Filled with a Porous Medium. *Sci. Rep.* **2017**, *7*, 2357. [CrossRef]

16. Chamkha, A.J.; Ismael, M. Natural Convection in Differentially Heated Partially Porous Layered Cavities Filled with a Nanofluid. *Numer. Heat Transf. Part A Appl.* **2014**, *65*, 1089–1113. [CrossRef]

17. Al-Srayyih, B.M.; Gao, S.; Hussain, S.H. Effects of linearly heated left wall on natural convection within a superposed cavity filled with composite nanofluid-porous layers. *Adv. Powder Technol.* **2019**, *30*, 55–72. [CrossRef]

18. Barnoon, P.; Toghraie, D.; Dehkordi, R.B.; Afrand, M. Two phase natural convection and thermal radiation of Non-Newtonian nanofluid in a porous cavity considering inclined cavity and size of inside cylinders. *Int. Commun. Heat Mass Transf.* **2019**, *108*, 104285. [CrossRef]

19. Jabbar, M.Y.; Ahmed, S.Y.; Hamazh, H.; Ali, F.H.; Khafaji, S.O.W. Effect of Layer Thickness on Natural Convection in a Square Enclosure Superposed by Nano-Porous and Non-Newtonian Fluid Layers Divided by a Wavy Permeable Wall. *Int. J. Mech. Mechatron. Eng.* **2019**, *19*, 3.

20. Chen, C.K.; Cho, C.C. Natural Convection in Wavy-Wall Cavities Filled with Power-Law Fluid. *Int. J. Mech. Mechatron. Eng.* **2014**, *8*, 1387–1391.

21. Kefayati, G.; Tang, H. MHD thermosolutal natural convection and entropy generation of Carreau fluid in a heated enclosure with two inner circular cold cylinders, using LBM. *Int. J. Heat Mass Transf.* **2018**, *126*, 508–530. [CrossRef]

22. Saleh, H.; Alsabery, A.I.; Hashim, I. Natural convection in polygonal enclosures with inner circular cylinder. *Adv. Mech. Eng.* **2015**, *7*, 1687814015622899. [CrossRef]

23. Massarotti, N.; Nithiarasu, P.; Zienkiewicz, O. Natural Convection in Porous Medium-Fluid Interface Problems: A Finite Element Analysis by Using the CBS Procedure. *Int. J. Numer. Methods Heat Fluid Flow* **2001**, *11*, 473–490. [CrossRef]

24. Gobin, D.; Goyeau, B.; Neculae, A.P. Convective Heat and Solute Transfer in Partially Porous Cavities. *Int. J. Heat Mass Transf.* **2005**, *48*, 1898–1908. [CrossRef]

25. Hirata, S.C.; Goyeau, B.; Gobin, D.; Carr, M.; Cotta, R. Linear Stability of Natural Convection in Superposed Fluid and Porous Layers: Influence of the Interfacial Modelling. *Int. J. Heat Mass Transf.* **2007**, *50*, 1356–1367. [CrossRef]

26. Aguilar-Madera, C.G.; Valdés-Parada, F.J.; Goyeau, B.; Ochoa-Tapia, J.A. One-Domain Approach for Heat Transfer Between a Porous Medium and a Fluid. *Int. J. Heat Mass Transf.* **2011**, *54*, 2089–2099. [CrossRef]

27. Aguilar-Madera, C.G.; Valdés-Parada, F.J.; Goyeau, B.; Ochoa-Tapia, J.A. Ochoa-Tapia, Convective Heat Transfer in a Channel Partially Filled with a Porous Medium. *Int. J. Therm. Sci.* **2011**, *50*, 1355–1368. [CrossRef]

28. Abu-Hijleh, B.; Al-Nimr, M. The Effect of the Local Inertial Term on the Fluid Flow in Channels Partially Filled with Porous Material. *Int. J. Heat Mass Transf.* **2001**, *44*, 1565–1572. [CrossRef]

29. Turan, O.; Sachdeva, A.; Chakraborty, N.; Poole, R.J. Laminar natural convection of power-law fluids in a square enclosure with differentially heated side walls subjected to constant temperatures. *J. Non-Newton. Fluid Mech.* **2011**, *166*, 1049–1063. [CrossRef]

30. Kefayati, G.; Tang, H.; Chan, A.; Wang, X. A lattice Boltzmann model for thermal non-Newtonian fluid flows through porous media. *Comput. Fluids* **2018**, *176*, 226–244. [CrossRef]

31. Akbal, S.; Baytaş, F. Effects of non-uniform porosity on double diffusive natural convection in a porous cavity with partially permeable wall. *Int. J. Therm. Sci.* **2008**, *47*, 875. [CrossRef]

32. Mchirgui, A.; Hidouri, N.; Magherbi, M.; Ben Brahim, A. Second law analysis in double diffusive convection through an inclined porous cavity. *Comput. Fluids* **2014**, *96*, 105–115. [CrossRef]

33. Bera, P.; Pippal, S.; Sharma, A.K. A thermal non-equilibrium approach on double-diffusive natural convection in a square porous-medium cavity. *Int. J. Heat Mass Transf.* **2014**, *78*, 1080–1094. [CrossRef]

34. Zhu, Q.; Zhuang, Y.; Yu, H. Three-dimensional numerical investigation on thermosolutal convection of power-law fluids in anisotropic porous media. *Int. J. Heat Mass Transf.* **2017**, *104*, 897–917. [CrossRef]

35. Kefayati, G. Simulation of double diffusive natural convection and entropy generation of power-law fluids in an inclined porous cavity with Soret and Dufour effects (Part I: Study of fluid flow, heat and mass transfer). *Int. J. Heat Mass Transf.* **2016**, *94*, 539–581. [CrossRef]

36. Kefayati, G. Simulation of double diffusive natural convection and entropy generation of power-law fluids in an inclined porous cavity with Soret and Dufour effects (Part II: Entropy generation). *Int. J. Heat Mass Transf.* **2016**, *94*, 582–624. [CrossRef]

37. Hussain, S.; Schieweck, F.; Turek, S. Effcient Newton multigrid solution techniques for higher order space time Galerkin discretizations of incompressible flow. *Appl. Numer. Math.* **2014**, *83*, 51–71. [CrossRef]

38. SHussain, S.; Mehmood, K.; Sagheer, M.; Farooq, A. Entropy generation analysis of mixed convective flow in an inclined channel with cavity with Al_2O_3-water nanofluid in porous medium. *Int. Commun. Heat Mass Transf.* **2017**, *89*, 198–210. [CrossRef]
39. Gibanov, N.S.; Sheremet, M.A.; Ismael, M.A.; Chamkha, A.J. Mixed convection in a ventilated cavity filled with a triangular porous layer. *Transp. Porous Media* **2017**, *89*, 198–210. [CrossRef]
40. Corvaro, F.; Paroncini, M. Experimental analysis of natural convection in square cavities heated from below with 2D-PIV and holographic interferometry techniques. *Exp. Therm. Fluid Sci.* **2007**, *31*, 721–739. [CrossRef]